



Extended phase matching of high harmonic generation by plasma-induced defocusing

HUNG-WEI SUN,^{1,†} PEI-CHI HUANG,^{1,2,†} YI-HSUAN TZENG,¹ JEN-TING HUANG,¹ C. D. LIN,^{3,4} CHENG JIN,^{5,6} AND MING-CHANG CHEN^{1,4,*}

¹Institute of Photonics Technologies, National Tsing Hua University, Hsinchu 30013, Taiwan

²Institute of Atomic and Molecular Sciences, Academia Sinica, Taipei 10617, Taiwan

³J. R. Macdonald Laboratory, Physics Department, Kansas State University, Manhattan, Kansas 66506-2604, USA

⁴Department of Physics, National Tsing Hua University, Hsinchu 30013, Taiwan

⁵Department of Applied Physics, Nanjing University of Science and Technology, Nanjing, Jiangsu 210094, China

⁶e-mail: cjin@njjust.edu.cn

*Corresponding author: mingchang@mx.nthu.edu.tw

Received 25 May 2017; revised 16 July 2017; accepted 18 July 2017 (Doc. ID 296779); published 11 August 2017

High-harmonic generation (HHG) of femtosecond lasers produces unique short-wavelength light pulses with femtosecond to attosecond duration. However, free electrons in the partially ionized gas medium are known to prevent phase matching and limit upconversion to low-energy harmonics only. We have demonstrated experimentally and theoretically an unconventional phase-matching scheme: extending the HHG phase matching cutoff by controlling the rapid self-defocusing effect of the driving laser. This method takes advantage of the additional intrinsic atomic dipole phase mismatch introduced by the rapid laser defocusing. This phase can be precisely controlled by adjusting the aperture of a simple iris, which truncates the input beam, to correctly compensate free-electron dispersion, resulting in tunable harmonic energy and phase matching cutoff extension. Based on this approach, we report experimental observation of extending the harmonic cutoff energy in Ar to ~ 65 eV with a 400-fold increase in conversion efficiency using a tightly focused truncated Gaussian beam in a short high-pressure gas cell. This new defocusing-assisted phase matching in a highly ionized gas medium can be applied to different targets, laser wavelengths, and pulse durations to extend harmonic upconversion to higher cutoff energy with higher efficiency. ©2017

Optical Society of America

OCIS codes: (190.0190) Nonlinear optics; (190.7110) Ultrafast nonlinear optics; (190.7220) Upconversion; (340.7480) X-rays, soft x-rays, extreme ultraviolet (EUV); (190.2620) Harmonic generation and mixing; (320.7120) Ultrafast phenomena.

<https://doi.org/10.1364/OPTICA.4.000976>

1. INTRODUCTION

The science and technology of ultrafast, coherent extreme-UV (EUV) lights have received a great deal of attention in recent years, especially in producing tabletop light sources through high-harmonic generation (HHG) processes. By focusing an intense laser beam into gaseous targets, a bound electron may be liberated into the continuum, which is then accelerated by the driving laser field to gain kinetic energy. As the field direction is reversed, the electron may be driven back to the mother ion and recombine to emit high-energy photons [1–3]. Through this upconversion process, light sources from EUV to soft x rays have been made available. However, most applications so far employed only relatively low-energy EUV wavelengths, because the efficiency of the HHG process drops rapidly at higher photon energies [4–7]. This decrease is not due to a lack of available laser intensity, but rather is due to the challenge of overcoming the large phase mismatch between the harmonics and the driving laser. A laser that generates harmonics also ionizes the medium,

where excessive free electrons cause defocusing and phase mismatch, limiting the nonlinear upconversion efficiency. For an 800 nm driving laser, the “critical” ionization level is $\eta_c \approx 3.8\%$ for Ar. This would lead to maximal cutoff energy near ~ 45 eV [8,9].

For ionization above the critical level, the free-electron dispersion cannot be compensated by the neutral atom dispersion. Overcoming this limitation to extend harmonic cutoff energy becomes a challenge. A variety of schemes have been proposed, such as quasi phase matching (QPM) [10–12], multi-jets [13–15], and short-pulse phase matching [16]. However, QPM and multi-jets require either the modulated geometry or the coherent combination of many lasers, while short-pulse phase matching requires a sophisticated laser system to produce few-cycle pulses. An alternative to extend the cutoff harmonic is to use a longer driving wavelength laser. However, at the single-atom level the efficiency scales like $\lambda^{-5.5}$ to $\lambda^{-6.5}$ [8,17–20]. While conversion efficiency can be improved by increasing the pressure in

the gas cell, the brightness of harmonics driven by long-wavelength lasers is still weaker than that driven by short-wavelength lasers [21].

In this work, we report that by adjusting the aperture size of an iris to control the truncation of a regular 25 fs, 800 nm driving laser on a tightly focused short high-pressure gas cell, we are able to shift the center of high-energy harmonics in Ar to about 65 eV with full optimization of backing pressure. We observed high flux and a wide range of tunable harmonics spanning from ≈ 35 to ≈ 70 eV. Compared with gas jet or waveguide geometry, we found that only tight focusing geometry with a short high-pressure cell would allow us to observe this cutoff extension while keeping a very similar conversion efficiency. A three-dimensional (3D) numerical model and advanced analysis enable us to explain this counterintuitive result: an extension of the phase-matching cutoff resulting from the plasma-induced defocusing effect. We refer to this new mechanism as defocusing-assisted phase matching (DAPM), which is one kind of nonadiabatic self-phase matching [22], but DAPM mainly relies on the plasma-induced defocusing effect. This is in contrast to conventional phase matching (CPM), which is restricted by a low ionization level in the gas cell. DAPM operates at high intensity, short gas cell length, and high pressure. Phase mismatch due to the copious free electrons is balanced by the change in high-harmonic phase initiated by the fast drop in the laser intensity over a short distance. By adjusting the aperture of the iris, good phase matching was found at the leading edge of the laser pulse at locations away from the center of the beam. We emphasize that the iris scheme may have already been applied and discussed in the many previous works regarding phase matching and spatial shaping of HHG [23–27]. However, this work for the first time (to our knowledge) shows that the iris scheme surprisingly extends the phase-matching cutoff in tight focusing and a short high-pressure cell geometry. The working mechanism is associated with the plasma-induced defocusing effect, which also has not been revealed yet.

2. EXPERIMENT

To verify the influence of plasma defocusing on the phase matching cutoff of HHG or DAPM, we prepared the experimental setup shown in Fig. 1. Three different geometries have been employed for direct comparison: (a) a 75 cm focus with a 1.2-mm-long gas cell, (b) a 30 cm focus with an 8-mm-long gas cell, and (c) a 30 cm focus with a 0.8-mm-long gas cell. We focused the same 25 fs, 600 μ J laser pulses at a wavelength of 800 nm into these three Ar-filled gas cells, where the input beam has a Gaussian intensity distribution ($M^2 < 1.2$) and a beam diameter W_0 of 8 mm. These gas cells all consist of acrylic tubing, through which two holes were drilled by the driving laser itself in order to minimize the loading of the vacuum system and also eliminate plasma-induced defocusing before the laser enters the cell. The lens was held by one translation stage to precisely control the focus relative to the gas cell. Additionally, we placed an iris 5 cm in front of the focal lens to truncate the fundamental beam. The optimization of the conversion efficiency, central energy, and maximum achievable photon energy is realized by adjusting the iris size, together with the focus position relative to the gas cell. Note that in the absence of gas and the iris, using a 30 cm focus, the focus diameter will be ≈ 45 μ m, resulting in a peak intensity of $\approx 3.6 \times 10^{15}$ W/cm², over a Rayleigh range of ≈ 2 mm. At such a high intensity, Ar is easily ionized, resulting in multiply

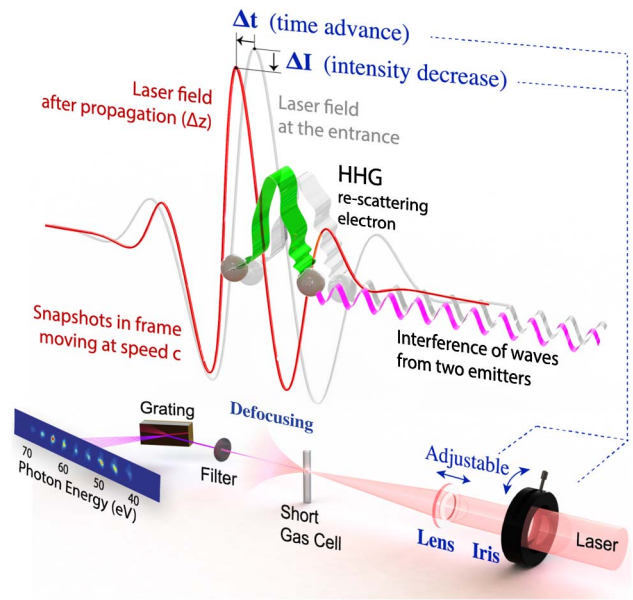


Fig. 1. Schematic of the experimental setup for defocusing-assisted phase matching. Operational phase matching is conveniently discovered by tuning the aperture size, together with the focus position with respect to the gas cell, to vary the $\Delta I/\Delta t$ ratio. See text for more details.

charged Ar ions (with an ionization level $> 300\%$) in the gas cell at the peak of the pulse based on the Ammosov–Delone–Krainov ionization model [28], while for the loosely 75 cm focus, the peak intensity $\approx 6 \times 10^{14}$ W/cm². It is clear that after entering the gas, dispersion due to the free electrons would modify the laser profile, especially for tight focusing geometry. When the pulse was interacting with the gas medium, the actual laser spot size and peak intensity were not determined. After the gas cell, the scattered laser light was blocked either by Al or a Zr filters, depending on the photon energy range under investigation. A set of KB mirrors was installed before the EUV grating (not shown in Fig. 1) to refocus harmonics in both the horizontal and vertical directions. The frequency response of the grating between 30 and 80 eV was almost uniform, which was calibrated by comparing the HHG spectrum with its time-of-flight photoelectron spectrum. Another important factor to increase the HHG flux would be to increase the backing pressure, since in free-focusing geometry, phase matching is only weakly dependent on pressure, as indicated in Fig. S2 of Supplement 1. By increasing the pressure, we maximized the brightness of the HHG until gas reabsorption took over (see Fig. S4 of Supplement 1).

Figure 2 shows that a short gas cell in tight focusing geometry offers several advantages. First, with a precisely controlled truncated beam, a short gas cell allows the extension of bright harmonics beyond the CPM cutoff, which is ≈ 45 eV for Ar. Second, it succeeds in enhancing conversion efficiency in the 65 eV region by more than 400 times. We also observed the harmonic signal below 50 eV scales with pressure as $P^{2.5}$, which is consistent with the conventional P^2 (phase-matched) HHG buildup. The harmonic flux near ≈ 65 eV, on the other hand, was found to scale as P^5 (Fig. S4 of Supplement 1), suggesting a different phase-matching mechanism. Third, a broad range of harmonics are generated in a short gas cell. The 8 mm cell generates a FWHM bandwidth of ≈ 6 eV at a center energy of 51 eV. In a

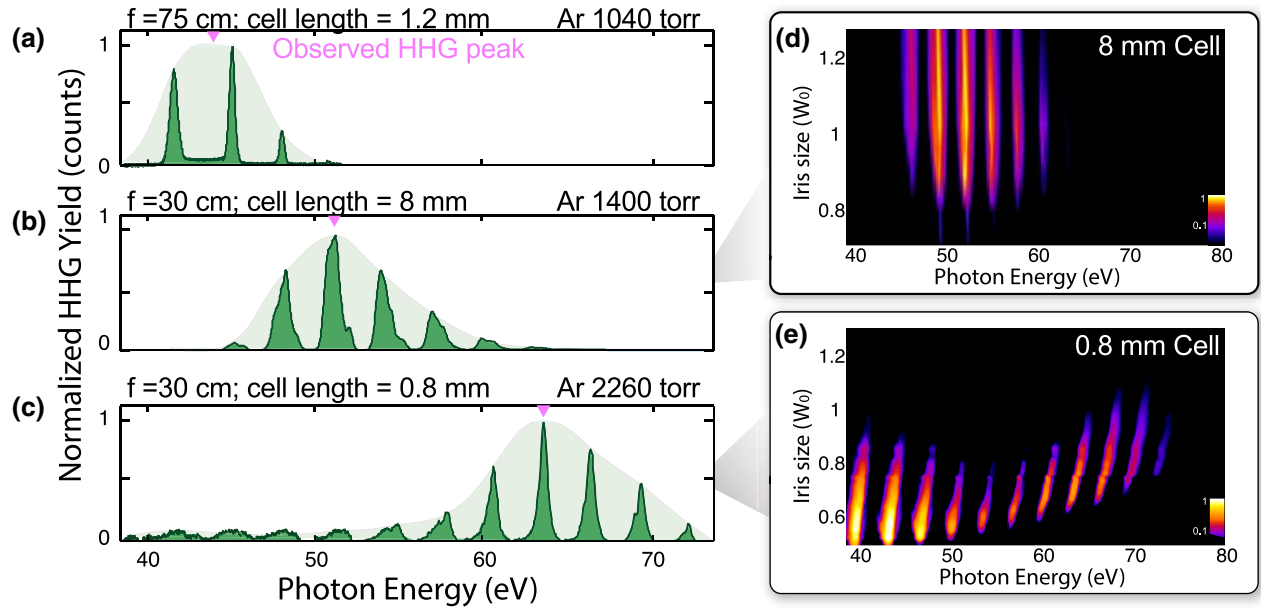


Fig. 2. Comparison of HHG spectrum obtained from three different experimental geometries. It shows that the combination of tight focusing and a short gas cell in (c) gives the highest observed photon energy. Each HHG spectrum in Ar shown here has been fully optimized, aiming for the brightest and highest achievable photon energy by tuning the iris size, backing pressure, and focus position relative to the gas cell. The observed phase-matching cutoff is marked by the inverted purple triangle. With the focal position fixed with respect to the gas cell, (d) and (e) show the HHG spectrum (log scale) versus different iris aperture sizes in the 8- and 0.8-mm-long gas cells, respectively. In (e), a suppression around 51 eV is due to the Cooper minimum of Ar.

0.8 mm gas cell, a 5 times broader bandwidth (FWHM: 35–67 eV) was observed. Finally, using a short gas cell, significant selectivity and tunability occurs when the iris aperture size is altered [Fig. 2(e)]. The center of the harmonic spectrum shifts continuously from 35 to 70 eV when the iris aperture size is varied from $0.45W_0$ to $0.9W_0$. We emphasize that to observe Fig. 2(c), a few optimization iterations are required to find the proper combination of iris aperture size and focus position relative to the cell. Such tunability is the consequence of plasma-defocusing-assisted phase matching, which is discussed in more detail below.

Qualitatively, Fig. 2 can be understood using an on-axis phase-matching model (discussed in Fig. S1 of Supplement 1). In the loosely focused case (75 cm focus) with a lower intensity, phase mismatch due to geometric phase and intrinsic dipole phase can be ignored. CPM works in Fig. 2(a). We can see the phase-matching cutoff energy at 45 eV, which is determined by the “critical” ionization level. In the tightly focused laser (30 cm focus), the dispersion due to free electrons would defocus the laser beam, decrease the laser intensity, and effectively reduce the Rayleigh range. However, we still observed bright harmonics at 70 eV, but the phase-matching zone was shorter when compared to the no-defocusing case. Therefore, we observed the extended cutoff energy of 70 eV in Fig. 2(c) only with a 0.8 mm gas cell. Next, we use analytic theory and an advanced numerical model to understand the main mechanism of how DAPM is achieved with the assistance of the defocusing effect.

3. THEORY

The expression for the q th-order harmonic phase with respect to the fundamental is given by [29], $\Phi_q = q\omega t_r - \int_{t_b}^{t_r} [(I_p + p^2/2m)/\hbar] dt$, where q is the harmonic order, t_b is the ionization time, t_r is the recombination time, I_p is the

ionization potential, and p is the canonical momentum. For high-order harmonics, where $p^2/2m \gg I_p$, the I_p term can be neglected and the electron kinetic energy is approximately equal to the emitted photon energy. The harmonic phase can be simplified to $\Phi_q \cong q\omega t_r - \theta_q^\Gamma I_L$, where Γ is the index of a specific trajectory. The coefficient θ_q^Γ depends highly on the trajectory and the harmonic order.

As illustrated in Fig. 1, there are two HHG emitters. One is excited by the laser at the entrance and the other occurs later inside the gas cell after the laser has propagated a distance Δz (subscripts 1 and 2 are used to identify them). The output of the q th harmonic relies on the $q\omega$ emitters interfering with each other. In the speed of the light frame, the HHG phase difference $\Delta\Phi_q$ between the two emitters is given by

$$\Delta\Phi_q = (\Phi_q)_2 - (\Phi_q)_1 \cong q\omega \underbrace{(t_{r_2} - t_{r_1})}_{=\Delta t} - \theta_q^\Gamma \underbrace{(I_{L_2} - I_{L_1})}_{=\Delta I}. \quad (1)$$

This would lead to a phase mismatch

$$\Delta k = \Delta\Phi_q / \Delta z \cong [q\omega \Delta t - \theta_q^\Gamma \Delta I] / \Delta z, \quad (2)$$

where Δt is the shift in time of the peak electric field and ΔI is the change in intensity over a propagation distance Δz [30]. All dispersion sources would influence Δt . Thus phase matching of each harmonic order is directly influenced by the dynamical evolution of the driving laser. In our experiment, by carefully truncating the laser beam to adjust the intensity and wavefront of the fundamental field entering the cell, the phase advance of the HHG field due to plasma and Gouy phase dispersion ($\Delta t / \Delta z$) can be compensated by the retardation of the HHG quantum phase caused by the defocusing gradient ($\Delta I / \Delta z$). This DAPM operates in a highly ionized gas medium, in contrast

with the CPM operating at a low ionization level with little change in the fundamental beam in the gas medium.

A consequence of DAPM is that it could selectively enhance a narrow bandwidth and further extend the HHG cutoff. Because the optimized defocusing gradient $\Delta I/\Delta z$ for compensating free electron and Gouy phase dispersion $\Delta t/\Delta z$ varies with the harmonic order q , phase matching occurs only when $\Delta I/\Delta t = q\omega/\theta_q^r$, as indicated by Eq. (2). This result agrees very well with our experimental observation, shown in Fig. 2(e). Enhancement of the harmonic spectra shifts to a higher order as the aperture size is increased. Since higher-energy harmonics are generated at higher intensities, a larger temporal phase mismatch $q\omega\Delta t/\Delta z$ is balanced by a stronger defocusing gradient $\theta_q^r\Delta I/\Delta z$. A proper $\Delta I/\Delta t$ ratio is created by a slightly larger iris size.

To better understand the spatiotemporal dynamics of the driving laser beam and iris-tuning phase matching, we performed 3D numerical macroscopic HHG simulations (see the method in Supplement 1). The parameters for the simulation were chosen to be close to those in the experiment. Figures 3(a)–3(c) compare the time–frequency representation of the harmonics as a function of the aperture size. At $0.37 W_0$, bright low-order ≈ 40 eV harmonics are dominant and are emitted symmetrically on both the rising and falling sides of the pulse. As the aperture is increased from $0.37 W_0$ to $0.40 W_0$, and then to $0.47 W_0$, [from Fig. 3(a) to Fig. 3(c)], the approximate 65 eV harmonic emerges at the front edge ($t \approx -3$ optical cycle) of the pulse but is off the center at $r \approx 10 \mu\text{m}$ of the beam axis (see Fig. S3 of Supplement 1), because the free-electron plasma severely defocuses the beam

near the center and the trailing edge of the pulse. With a longer propagation distance [Fig. 3(d)], ionization-induced defocusing further limits the laser peak intensity such that it is not intense enough to produce the 65 eV harmonic. The same simulation also shows that the ≈ 40 eV harmonic occurs mainly at laser peak $t \approx 0$ optical cycle and near the center, $r \approx 0 \mu\text{m}$.

Figure 3(e) demonstrates the growth of 42.8 and 64.7 eV harmonics versus the propagation distance at the same input pulse energy. Clearly there are two kinds of phase matching at work. The first kind is the one for the 42.8 eV harmonic shown in Fig. 3(d), where the harmonic is generated near the end of the cell. At the beginning of the cell, the laser intensity is too high for phase matching to work. As the driving laser pulse propagates over a certain distance, its intensity is reduced such that the CPM becomes possible (ionization level $< 3.8\%$) and the pulse is naturally shaped into a gentle focusing to allow for a much longer distance for the effective generation of the 42.8 eV harmonic, as shown in Fig. 3(f). An equivalent result has been obtained in Ref. [31] by employing temporal pulse shaping. In such CPM, the cutoff energy in Ar is 45 eV. The simulation illustrates that after a few millimeters of propagation, the change in the laser field becomes small and allows low harmonics to build up, and harmonics are generated near the axis.

The harmonics observed near 65 eV are due to DAPM. Figure 3(e) shows that these harmonics are generated at the beginning of an ≈ 1 mm cell, but further propagation reduces their final yields. Thus they would be observed for a short gas cell only, such as the 0.8 mm cell seen in Fig. 3(c), and in the experimental data [see Figs. 2(c) and 2(e)]. Figure 3(g) shows

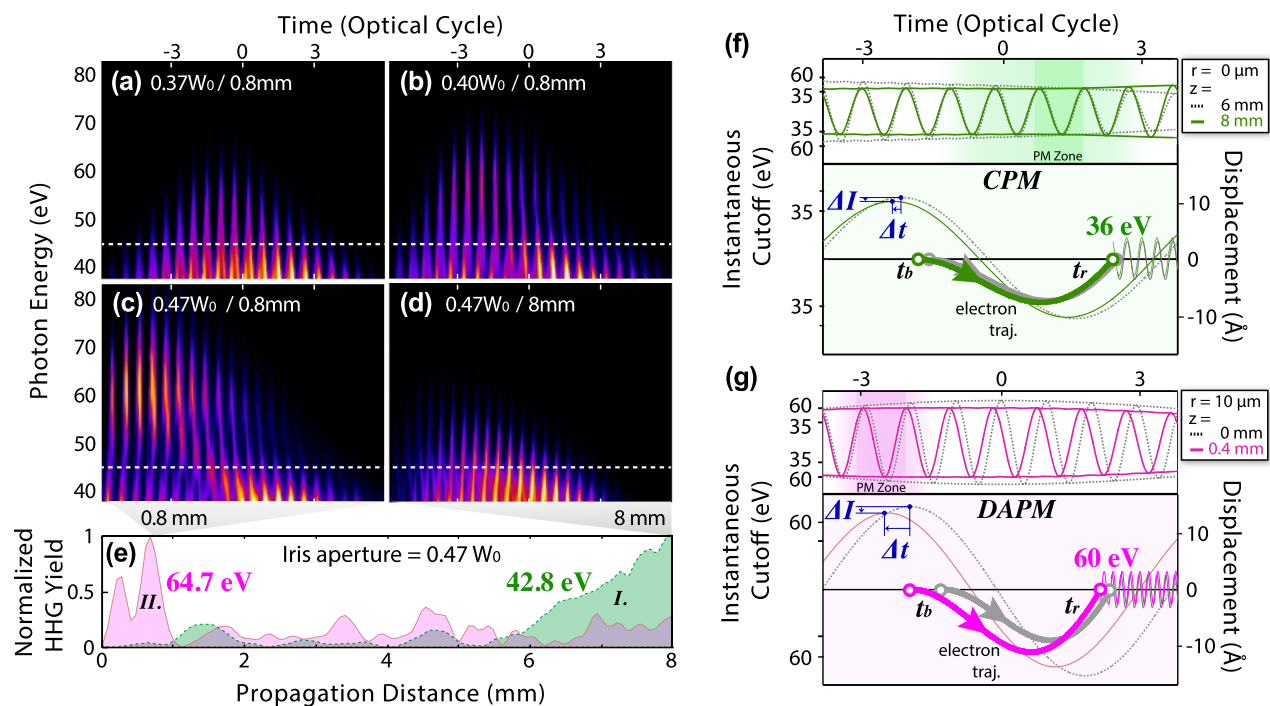


Fig. 3. Time–frequency analysis of HHG emission from a 10-cycle laser field is shown for the truncated beams of (a) $0.37W_0$, (b) $0.40W_0$, and (c) $0.47W_0$ with an 0.8 mm propagation and (d) $0.47W_0$ with an 8 mm propagation in a 50 torr Ar cell. The horizontal line marks the conventional phase-matching cutoff. (e) At $0.47W_0$, the yield of the 64.7 eV (42.8 eV) harmonic as a function of propagation distance, (f) the electric field at a propagation distance of $z = 6$ mm and $z = 8$ mm in the cell, together with the phase-matching zone and the corresponding electron re-scattering trajectories for the 36 eV harmonics, (g) similar plots to (f), but for the off-center position $r = 10 \mu\text{m}$, $z = 0.0$ – 0.4 mm, and for the 60 eV harmonic. These results are obtained by solving the three-dimensional Maxwell's equations for both the fundamental laser and the high-harmonic field.

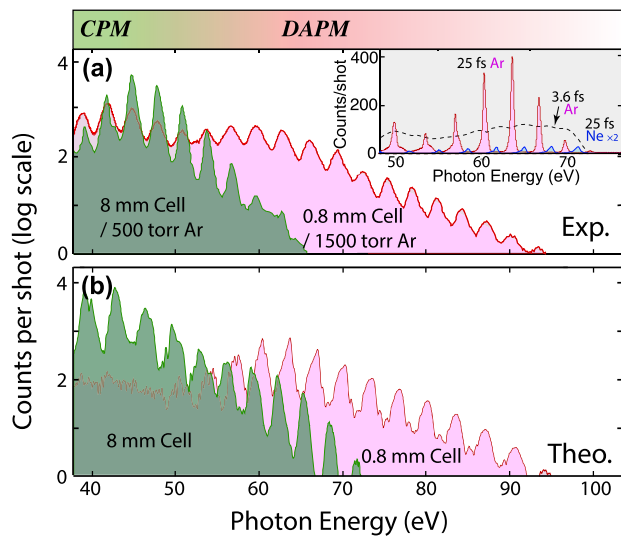


Fig. 4. (a) Comparison of the brightness of fully optimized HHG using 8 mm and 0.8 mm gas cells (CPM and DAPM, respectively), together with (b) the theoretical calculation. Inset: Comparison of HHG from Ar and Ne driven by multicycle pulses (red and blue lines, respectively), and Ar driven by few-cycle pulses (black dash) [33].

how transient DAPM is accomplished at a position off the center ($r = 10 \mu\text{m}$) for $z = 0.0$ and 0.4 mm. This occurs only when $\Delta I/\Delta z < 0$. The large shift in ΔI and Δt can be seen in this DAPM in Fig. 3(g). In DAPM, neutral-atom dispersion does not play the main role; it is reached when the Gouy phase and free-electron dispersion ($\Delta t/\Delta z$) are balanced by the harmonic phase induced by laser defocusing ($\Delta I/\Delta z$). As we observed in Fig. 2(e), this intrinsic phase can be precisely controlled by adjusting the aperture of a simple iris to correctly compensate the Gouy phase and free-electron dispersion, resulting in tunable harmonic energy and cutoff extension.

How does the brightness of the harmonics generated with DAPM matching compare with that using CPM? Using 8- and 0.8-mm-long gas cells, the HHG yield has been systematically optimized by varying parameters such as driving laser intensity, focal length, backing pressure of the gas cell, and aperture size, together with the focus position with respect to the gas target. Figure 4(a) compares the optimized yield of harmonics using the 8-mm-long cell, CPM, with the optimized yield of harmonics using the 0.8-mm-short cell, DAPM. Figure 4(b) displays the simulation results. With the 0.8 mm cell, the maximum flux at 65 eV is $\approx 4 \times 10^2$ counts per shot per pixel directly detected by one EUV CCD camera (Andor iKon), corresponding to $\approx 3.2 \times 10^9$ photons per second (1 kHz) for one single 41st order (≈ 65 eV), after correcting for the known CCD quantum efficiency, grating efficiency, and filter transmission. This flux is more than ≈ 400 times larger than the long gas cell value at the same wavelength. But at 45 eV, the long cell is about 5 times brighter than the short cell. Note that based on this broadband and high flux source at 65 eV we have for the first time (to our knowledge) developed an EUV scatterometer, for determining nanoscale structural parameters of a period silicon array [32].

In the inset of Fig. 4(a), the present harmonics around 65 eV are compared to the optimized harmonics generated by 25 fs pulses in Ne and 3.6 fs pulses in Ar, by varying the focal length

(10–100 cm), gas cell length (0.8–12 mm), and driving laser intensity. Operationally the aperture size, the focus position, and the gas pressure have also been adjusted to reach the optimal harmonic yields. For the brightest 65 eV HHG in Ne driven by 25 fs pulses, the experiment used a 30 cm lens to focus 0.5 mJ pulses into one 1.2-mm-long gas cell. The optimized 65 eV harmonic from Ar reported here is more than ≈ 30 times brighter than that generated from Ne. For the brightest EUV continuum driven by few-cycle (3.6 fs) pulses, the maximum pulse energy is limited to 70 μJ , and the best geometry that has been found used a 15 cm focus length, together with one 1.2-mm-long gas cell [33]. The flux produced by DAPM is also slightly higher than that driven by few-cycle pulses.

4. CONCLUSION

We demonstrated experimentally and theoretically that intense high-energy harmonics near 65 eV can be obtained from Ar using an 800 nm laser in a tightly focused short gas cell under high pressure. When optimized, these harmonics have energy beyond the conventional cutoff of about 45 eV, with hundreds of times higher brightness, which is also brighter than harmonics that are generated from neon atoms or driven by few-cycle pulses. Such intense light in this spectral region represents a substantial increase in the influence of nano-imaging, and of ultrafast element-selective magneto-optic experiments, e.g., M-shell absorption edges of Co, Fe, and Ni. Theoretical analysis reveals that a dynamic phase-matching mechanism, DAPM, is at work where the defocusing, caused by the excessive free electrons, induces an additional intrinsic quantum phase as the driving laser travels through the medium, to help compensate the phase mismatch. This mechanism helps in the observation of extending the harmonic cutoff. Experimentally the optimal phase-matching conditions can be reached by tuning the aperture of the iris. Based on DAPM, one can also dial up for high brightness harmonics in different spectral regions for different experimental needs. While the experiment was carried out only for an Ar target and 800 nm laser, the method can be extended to other targets and lasers of different wavelengths and pulse durations.

Funding. Ministry of Science and Technology, Taiwan (MOST) (105-2112-M-007-030-MY3); Fundamental Research Funds for the Central Universities of China (30916011207); U.S. Department of Energy (DOE) (DE-FG02-86ER13491); Air Force Office of Scientific Research (AFOSR) (FA9550-14-1-0255).

Acknowledgment. The experimental work was done at NTHU IPT, supported by the Ministry of Science and Technology, Taiwan. C. J. was supported by Fundamental Research Funds for the Central Universities of China. C. D. L. was supported by the Chemical Sciences, Geosciences and Biosciences Division, Office of Basic Energy Sciences, Office of Science, U.S. Department of Energy, and by the U.S. Air Force Office of Scientific Research. The authors would like to thank Dr. Andy Kung for providing us a femtosecond laser system.

[†]These authors contributed equally to this work.

See Supplement 1 for supporting content.

REFERENCES

1. A. L'Huillier, K. J. Schafer, and K. C. Kulander, "Theoretical aspects of intense field harmonic-generation," *J. Phys. B* **24**, 3315–3341 (1991).
2. P. B. Corkum, "Plasma perspective on strong-field multiphoton ionization," *Phys. Rev. Lett.* **71**, 1994–1997 (1993).
3. M. Lewenstein, P. Balcou, M. R. Y. Ivanov, A. L'Huillier, and P. B. Corkum, "Theory of high-harmonic generation by low-frequency laser fields," *Phys. Rev. A* **49**, 2117–2132 (1994).
4. Z. Tao, C. Chen, T. Szilvasi, M. Keller, M. Mavrikakis, H. Kapteyn, and M. Murnane, "Direct time-domain observation of attosecond final-state lifetimes in photoemission from solids," *Science* **353**, 62–67 (2016).
5. G. Sansone, F. Kelkensberg, J. F. Pérez-Torres, F. Morales, M. F. Kling, W. Siu, O. Ghafur, P. Johnsson, M. Swoboda, E. Benedetti, F. Ferrari, F. Lépine, J. L. Sanz-Vicario, S. Zherebtsov, I. Znakovskaya, A. L'Huillier, M. Y. Ivanov, M. Nisoli, F. Martin, and M. J. J. Vrakking, "Electron localization following attosecond molecular photoionization," *Nature* **465**, 763–766 (2010).
6. V. Gruson, L. Barreau, Á. Jiménez-Galan, F. Risoud, J. Caillat, A. Maquet, B. Carré, F. Lepetit, J.-F. Hergott, T. Ruchon, L. Argenti, R. Taïeb, F. Martín, and P. Salieres, "Attosecond dynamics through a Fano resonance: Monitoring the birth of a photoelectron," *Science* **354**, 734–738 (2016).
7. C. La-O-Vorakiat, M. Siemens, M. M. Murnane, H. C. Kapteyn, S. Mathias, M. Aeschlimann, P. Grychtol, R. Adam, C. M. Schneider, J. M. Shaw, H. Nembach, and T. J. Silva, "Ultrafast demagnetization dynamics at the M edges of magnetic elements observed using a tabletop high-harmonic soft x-ray source," *Phys. Rev. Lett.* **103**, 257402 (2009).
8. T. Popmintchev, M.-C. Chen, A. Bahabad, M. Gerrity, P. Sidorenko, O. Cohen, I. P. Christov, M. M. Murnane, and H. C. Kapteyn, "Phase matching of high harmonic generation in the soft and hard X-ray regions of the spectrum," *Proc. Natl. Acad. Sci. USA* **106**, 10516–10521 (2009).
9. E. J. Takahashi, T. Kanai, Y. Nabekawa, and K. Midorikawa, "10 mJ class femtosecond optical parametric amplifier for generating soft x-ray harmonics," *Appl. Phys. Lett.* **93**, 041111 (2008).
10. E. A. Gibson, A. Paul, N. Wagner, D. Gaudiosi, and S. Backus, "Coherent soft x-ray generation in the water window with quasi-phase matching," *Science* **302**, 95–98 (2003).
11. X. Zhang, A. L. Lytle, T. Popmintchev, X. Zhou, H. C. Kapteyn, M. M. Murnane, and O. Cohen, "Quasi-phase-matching and quantum-path control of high-harmonic generation using counterpropagating light," *Nat. Phys.* **3**, 270–275 (2007).
12. P. Sidorenko, M. Kozlov, A. Bahabad, T. Popmintchev, M. Murnane, H. Kapteyn, and O. Cohen, "Sawtooth grating-assisted phase-matching," *Opt. Express* **18**, 22686–22692 (2010).
13. J. Seres, V. S. Yakovlev, E. Seres, C. Strelli, P. Wobrauschek, C. Spielmann, and F. Krausz, "Coherent superposition of laser-driven soft-X-ray harmonics from successive sources," *Nat. Phys.* **3**, 878–883 (2007).
14. F. Brizuela, C. M. Heyl, P. Rudawski, D. Kroon, L. Rading, J. M. Dahlström, J. Mauritsson, P. Johnsson, C. L. Arnold, and A. L'Huillier, "Efficient high-order harmonic generation boosted by below-threshold harmonics," *Sci. Rep.* **3**, 1410 (2013).
15. A. Willner, F. Tavella, M. Yeung, T. Dzelzainis, C. Kamperidis, M. Bakarezos, D. Adams, M. Schulz, R. Riedel, M. C. Hoffmann, W. Hu, J. Rossbach, M. Drescher, N. A. Papadogiannis, M. Tatarakis, B. Dromey, and M. Zepf, "Coherent control of high harmonic generation via dual-gas multijet arrays," *Phys. Rev. Lett.* **107**, 175002 (2011).
16. J. Seres, E. Seres, A. J. Verhoef, G. Tempea, C. Strelli, P. Wobrauschek, V. Yakovlev, A. Scrinzi, C. Spielmann, and F. Krausz, "Laser technology: source of coherent kiloelectronvolt X-rays," *Nature* **433**, 596 (2005).
17. T. Popmintchev, M.-C. Chen, D. Popmintchev, P. Arpin, S. Brown, S. Alisauskas, G. Andriukaitis, T. Balčiūnas, O. D. Muecke, A. Pugzlys, A. Baltuška, B. Shim, S. E. Schrauth, A. Gaeta, C. Hernández-García, L. Plaja, A. Becker, A. Jaron-Becker, M. M. Murnane, and H. C. Kapteyn, "Bright coherent ultrahigh harmonics in the keV x-ray regime from mid-infrared femtosecond lasers," *Science* **336**, 1287–1291 (2012).
18. M.-C. Chen, P. Arpin, T. Popmintchev, M. Gerrity, B. Zhang, M. Seaberg, D. Popmintchev, M. M. Murnane, and H. C. Kapteyn, "Bright, coherent, ultrafast soft x-ray harmonics spanning the water window from a tabletop light source," *Phys. Rev. Lett.* **105**, 173901 (2010).
19. A. D. Shiner, C. Trallero-Herrero, N. Kajumba, H. C. Bandulet, D. Comtois, F. Légaré, M. Giguère, J. C. Kieffer, P. B. Corkum, and D. M. Villeneuve, "Wavelength scaling of high harmonic generation efficiency," *Phys. Rev. Lett.* **103**, 073902 (2009).
20. E. J. Takahashi, T. Kanai, K. L. Ishikawa, Y. Nabekawa, and K. Midorikawa, "Coherent water window x ray by phase-matched high-order harmonic generation in neutral media," *Phys. Rev. Lett.* **101**, 253901 (2008).
21. D. Popmintchev, C. Hernández-García, F. Dollar, C. Mancuso, J. A. Pérez-Hernández, M.-C. Chen, A. Hankla, X. Gao, B. Shim, A. L. Gaeta, M. Tarazkar, D. A. Romanov, R. J. Levis, J. A. Gaffney, M. Ford, S. B. Libby, A. Jaron-Becker, A. Becker, L. Plaja, M. M. Murnane, H. C. Kapteyn, and T. Popmintchev, "Ultraviolet surprise: efficient soft x-ray high-harmonic generation in multiply ionized plasmas," *Science* **350**, 1225–1231 (2015).
22. M. Geissler, G. Tempea, and T. Brabec, "Phase-matched high-order harmonic generation in the nonadiabatic limit," *Phys. Rev. A* **62**, 033817 (2000).
23. S. Kazamias, F. Weihe, D. Douillet, C. Valentin, T. Planchon, S. Sebban, G. Grillon, F. Augé, D. Hulin, and P. Balcou, "High order harmonic generation optimization with an apertured laser beam," *Eur. Phys. J. D* **21**, 353–359 (2002).
24. M. Turner, N. Brimhall, M. Ware, and J. Peatross, "Simulated laser-pulse evolution for high-order harmonic generation in a semi-infinite gas cell," *Opt. Express* **16**, 1571–1576 (2008).
25. V. V. Strelkov, E. Mével, and E. Constant, "Generation of isolated attosecond pulses by spatial shaping of a femtosecond laser beam," *New J. Phys.* **10**, 083040 (2008).
26. A. Dubrouil, O. Hort, F. Catoire, D. Descamps, S. Petit, E. Mével, V. V. Strelkov, and E. Constant, "Spatio-spectral structures in high-order harmonic beams generated with terawatt 10-fs pulses," *Nat. Commun.* **5**, 4637 (2014).
27. M. Nisoli, E. Priori, G. Sansone, S. Stagira, and G. Cerullo, "High-brightness high-order harmonic generation by truncated Bessel beams in the sub-10-fs regime," *Phys. Rev. Lett.* **88**, 033902 (2002).
28. M. V. Ammosov, N. B. Delone, and V. P. Krainov, "Tunnel ionization of complex atoms and of atomic ions in an alternating electric field," *J. Exp. Theor. Phys.* **91**, 2008–2013 (1986).
29. P. Balcou, P. Salieres, A. L'Huillier, and M. Lewenstein, "Generalized phase-matching conditions for high harmonics: the role of field-gradient forces," *Phys. Rev. A* **55**, 3204–3210 (1997).
30. C. Jin and C. D. Lin, "Spatially coherent high-order harmonics generated at optimal high gas pressure with high-intensity one- or two-color laser pulses," *Phys. Rev. A* **94**, 043804 (2016).
31. O. Boyko, C. Valentin, B. Mercier, C. Coquelet, V. Pascal, E. Papalazarou, G. Rey, and P. Balcou, "Systematic study of high-order harmonic optimal control by temporal pulse shaping of laser pulses," *Phys. Rev. A* **76**, 063811 (2007).
32. Y.-S. Ku, C.-L. Yeh, Y.-C. Chen, C.-W. Lo, W.-T. Wang, and M.-C. Chen, "EUV scatterometer with a high-harmonic-generation EUV source," *Opt. Express* **24**, 28014–28025 (2016).
33. P.-C. Huang, C.-H. Lu, B.-H. Chen, S.-D. Yang, M.-C. Chen, and A. H. Kung, "EUV continuum from compressed multiple thin plate supercontinuum," in *Conference on Lasers and Electro-Optics (CLEO) (Optical Society of America, 2016)*, paper FTU3N.7.